

# Supporting information for “From haemoglobin to single-site hydrogenation catalyst”

Alain Y. Li,<sup>a</sup> Angus Pedersen,<sup>a,b</sup> Jingyu Feng,<sup>a</sup> Hui Luo,<sup>a</sup> Jesús Barrio,<sup>a,b</sup> Julien Roman<sup>a</sup> King Kuok (Mimi) Hii,<sup>c</sup> Maria-Magdalena Titirici<sup>a,d\*</sup>

- Department of Chemical Engineering, Imperial College London, Exhibition Road, London SW7 2AZ
- Department of Materials, Royal School of Mines, Imperial College London, Exhibition Road, London SW7 2AZ, England, UK
- Department of Chemistry, Imperial College London, Molecular Sciences Research Hub, 80, Wood Lane, London W12 0BZ, U.K
- Advanced Institute for Materials Research (WPI-AIMR), Tohoku University, 2-1-1 Katahira, Aobaku, Sendai, Miyagi 980-8577, Japan
- 

Included in this document: Protocol for FeN<sub>x</sub>@C preparation, comments on ICP-MS results, EPR settings, HAADF-STEM and SEM details with additional images, fitting parameters and settings for XAS, XRD, Raman, XPS, BET details. Protocol for catalytic tests, catalyst recycling, comments on water traces, and notes on mechanism.

## Contents

Experimental section.....	1
1-Material synthesis.....	1
2-Characterisation.....	1
3-Catalysis.....	16
4-NMR spectra.....	18

## Experimental section.

All chemicals were purchased from Sigma Aldrich and used as received unless noted.

### 1-Material synthesis

**Hydrothermal treatment.** Hemoglobin (3.3 g, 15 wt%, Sigma-Aldrich, from bovine blood), xylose (18.7 g, 85 wt%), kayexalate (112 mg, 0.5 wt%) were manually stirred with a glass rod for 1 minute in a Teflon liner (100 mL) with distilled water (70 mL), then magnetically stirred at room temperature for 1 h until total dissolution of the solids. The liner was transferred to a stainless-steel autoclave (Parr Instrument) and heated at 220°C for 12 h (heating rate 10°C/min). After cooling down to room temperature, the resulting solid was filtered, rinsed three times with distilled water (1 L total), ethanol then acetone until the filtrate came out colorless, then dried overnight at 80°C. The resulting dark brown powder was ground using a mortar and pestle, with a few drops of acetone to assist the grinding.

**Pyrolysis.** The HTC carbon powder (3.0 g) was placed in a ceramic crucible (10\*3.3\*1.5 cm, 50 cm<sup>3</sup> total), covered with a ceramic lid and placed in a tube furnace followed by 15 min of flushing with an N<sub>2</sub>/O<sub>2</sub> mixture (6 % oxygen content, using compressed air as the oxygen source, 300 mL/min overall). The sample was then heated at a heating rate of 7 °C/min up to 1000 °C, with a dwell time of 2 h and subsequent cooling to room temperature (GHA-12-300 from Carbolite). The resulting black powder was then ground with a mortar and pestle and dried overnight at 80°C. Pyrolysis yield was 1.18 g (39%).

### 2-Characterisation

Entry	Catalyst	Fe concentration (ppm)	Specific surface area (m <sup>2</sup> /g)	Turnover frequency (10 <sup>3</sup> .h <sup>-1</sup> )	
1	Before pyrolysis	1600	40	0	
2	Oxygen % during pyrolysis	0	70	0	
3		2	360	80	
4		4	3200	530	720
5		6	4000	740 (610 <sup>[a]</sup> )	770
6		8	3300	640	250
7		10	370	680	110

**Table S1.** Iron titration and surface area data for the various materials prepared <sup>[a]</sup>surface area without the kayexalate template.

Pyrolysed samples (40 mg) were degassed at 200°C for 16 h before measurement (120°C for non-pyrolysed carbons). Nitrogen sorption isotherms were conducted at -196 °C in Micromeritics Tristar system. BET specific surface area was deduced from an analysis of the isotherm in the relative pressure range of 0.0002–0.03. The pore size distribution was calculated by HS-2D-NLDFT Carbon N<sub>2</sub> 77 method from Micromeritics, using the part of the isothermal data.

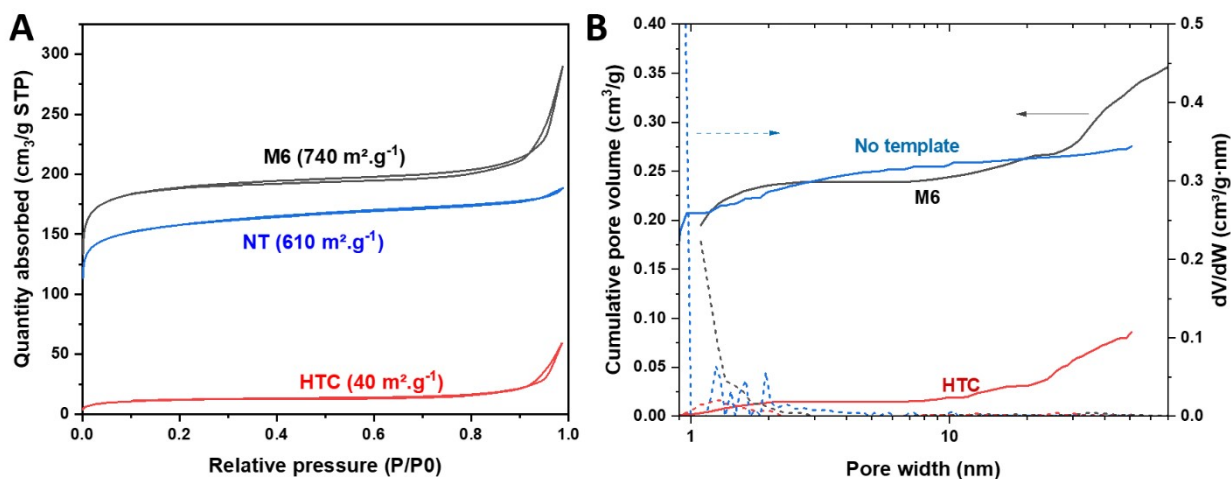


**Figure S1.** A) N<sub>2</sub> adsorption-desorption isotherm and B) Cumulative pore volume distributions for samples with different oxygen percentages during pyrolysis (M6: catalyst at 6% oxygen treatment, NT: catalyst without the kayexalate template, HTC: sample before pyrolysis).

**Inductively coupled plasma mass spectrometry (ICP-MS)** was obtained using an Agilent 7900 spectrometer (Agilent Technologies). ICP-MS samples were first digested in 69% HNO<sub>3</sub> (Certified AR, Eur.Ph., for analysis Fisher Chemical™, Fisher Scientific) by employing a MARS 6 microwave at 1500 W for 15 min at 215 °C. The resulting solutions were diluted to 2% HNO<sub>3</sub> and filtered for measurement against calibration standards containing Fe concentrations of 0, 5, 50, 100, 200, 500 ppb.

No catalytically active transition metal other than Fe was detected in measurable amounts (in particular Cr, Mn, Co, Ni, Mo, Ru, Rh, Pd, Ag, Ir, Pt, Au). ICP-MS showed that  $K_2CO_3$  contained 2000 ppm of Fe. In the standard conditions, this corresponds to 0.23 mol% Fe relative to the substrate (88  $\mu$ mol) or 6 mol% Fe relative to the  $FeN_x$  sites contained in the catalyst (3.5  $\mu$ mol). However, the control reaction without the catalyst gave no yield (Table 3, entry 4), showing that the Fe species contained in  $K_2CO_3$  is not catalytically active.  $KCO_2H$  did not show any Fe traces by ICP-MS.

**Continuous wave electron paramagnetic resonance (EPR)** was measured using an X-band CW ELEXSYS E500 EPR spectrometer (Bruker, Germany) with a cryogen-free variable temperature cryostat (Oxford Instruments, Oxfordshire, UK).  $\approx 3$  mg of sample (except for the empty tube measurement) was added to a 3 mm Wilmad quartz (CFQ) EPR tubes (Sigma Aldrich). Spectra were obtained at 5 K and 9.716 GHz with 20 mW incident microwave power, 100 kHz modulation frequency, 1 G modulation amplitude, and with magnetic field sweeping in 0.5 Gauss increments from 50 to 5000 Gauss.

**Scanning Transmission Electron Microscopy (HAADF-STEM)** was carried out for the imaging of single Fe atoms in a JEOL ARM200F at 200 kV and the images were analysed with Gatan software. STEM samples were dry-deposited onto the grids to avoid solvent contamination. Briefly, 5 mg of powder and a lacey carbon mesh copper grids (Agar Scientific, Lacey carbon film 400 Cu) were placed in a glass vial, followed by gentle shaking to enable the catalyst to attach onto the grid electrostatically. The grid was then picked up and shaken with a tweezer to remove the excess powder on the surface and stored in dry conditions.

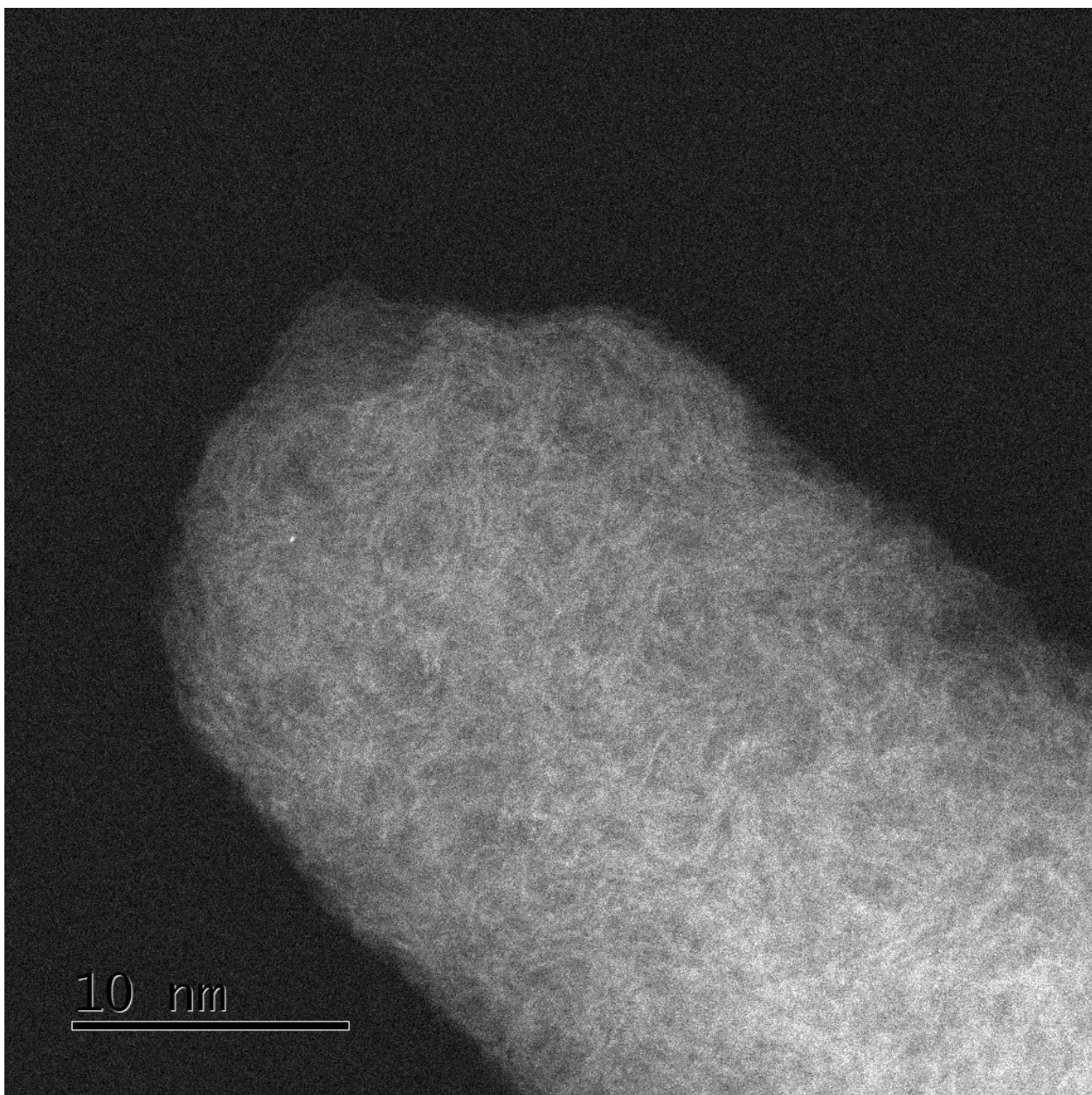


**Figure S2.** HAADF-STEM picture of the fresh catalyst.

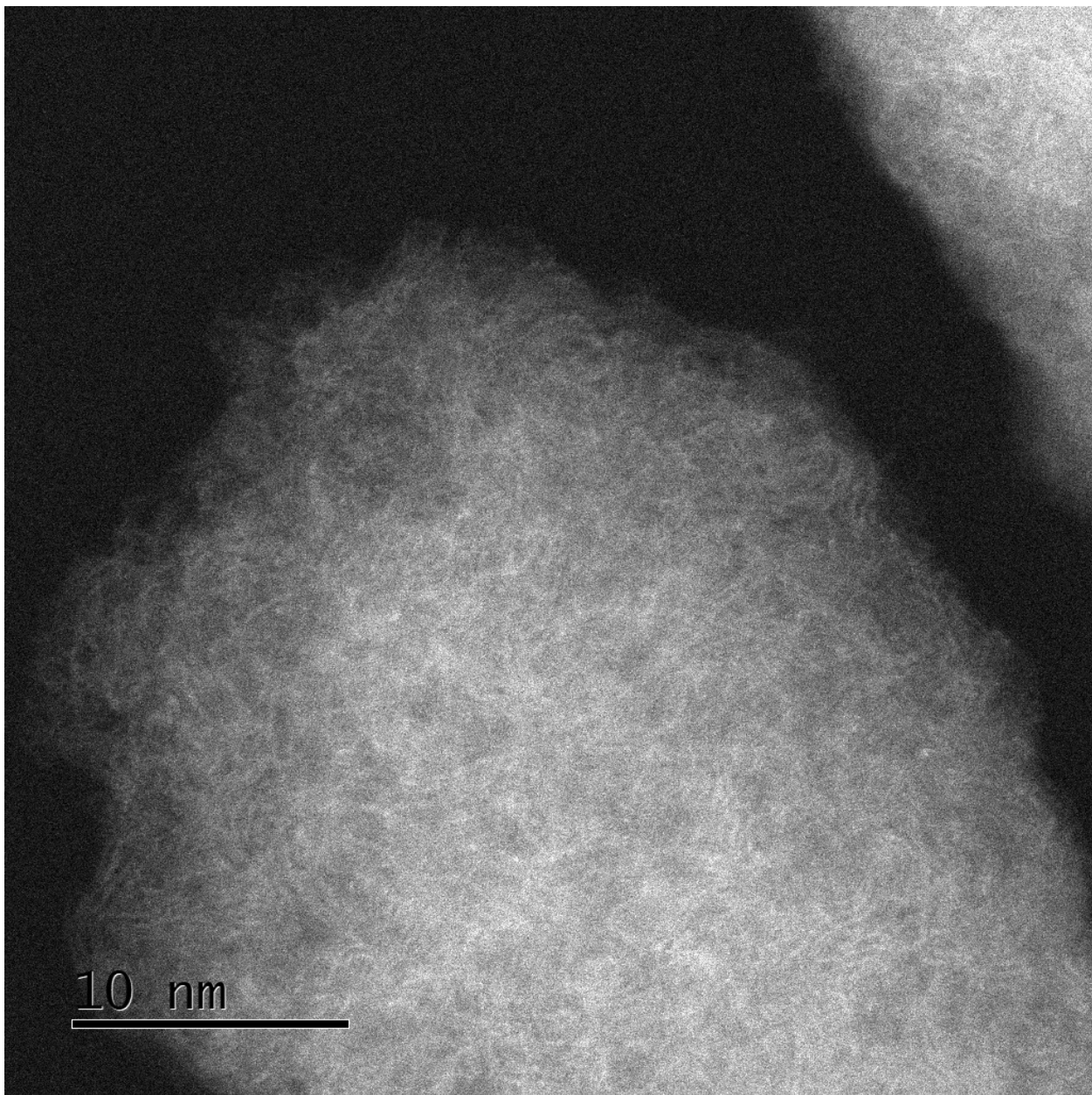


**Figure S3.** HAADF-STEM picture of the fresh catalyst.

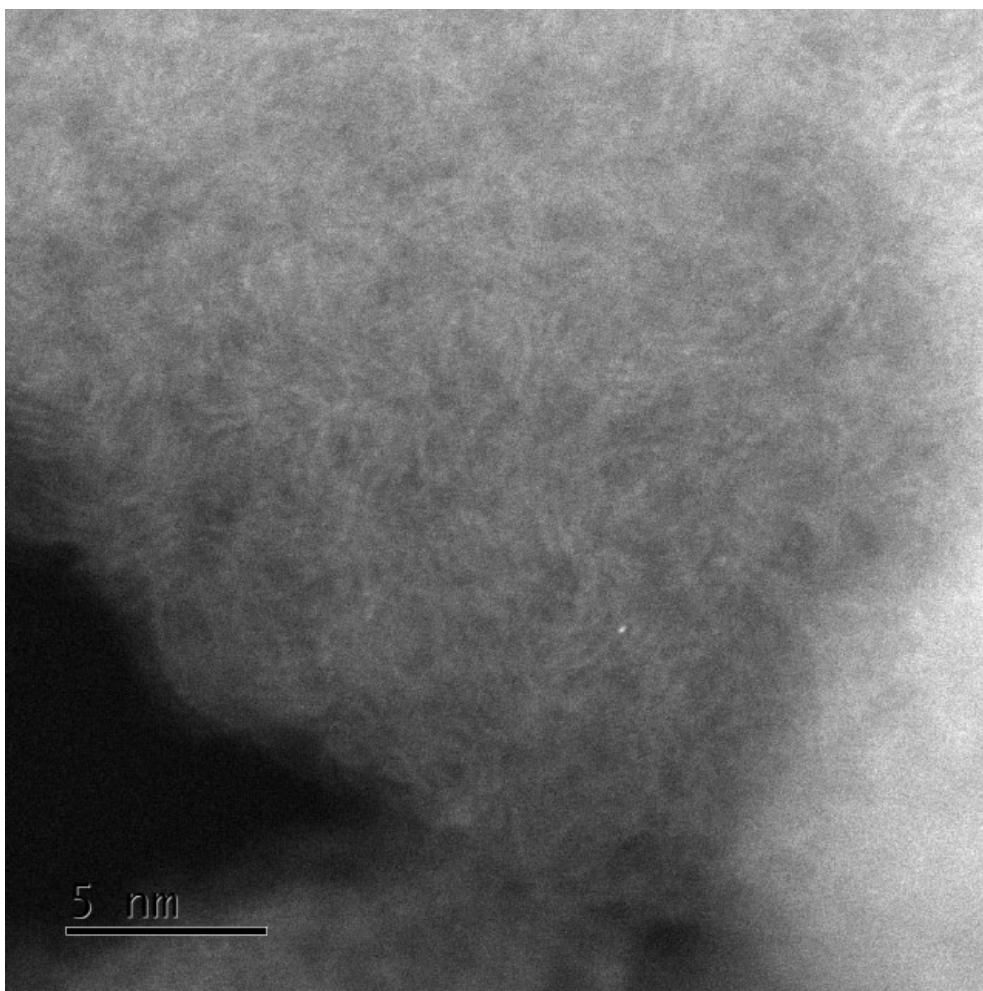


**Figure S4.** HAADF-STEM picture of the fresh catalyst.

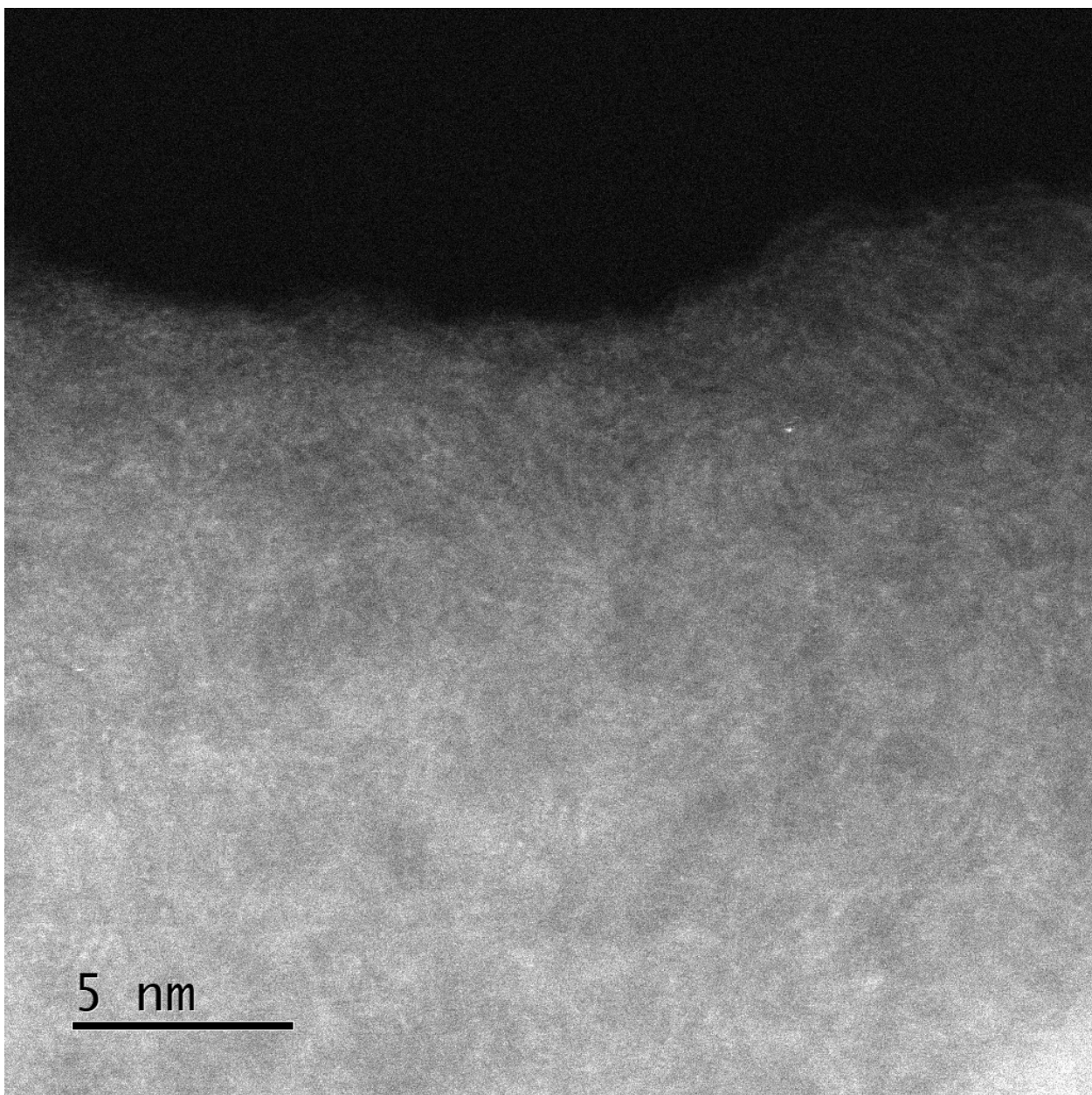


**Figure S5.** HAADF-STEM image of the catalyst after reaction.

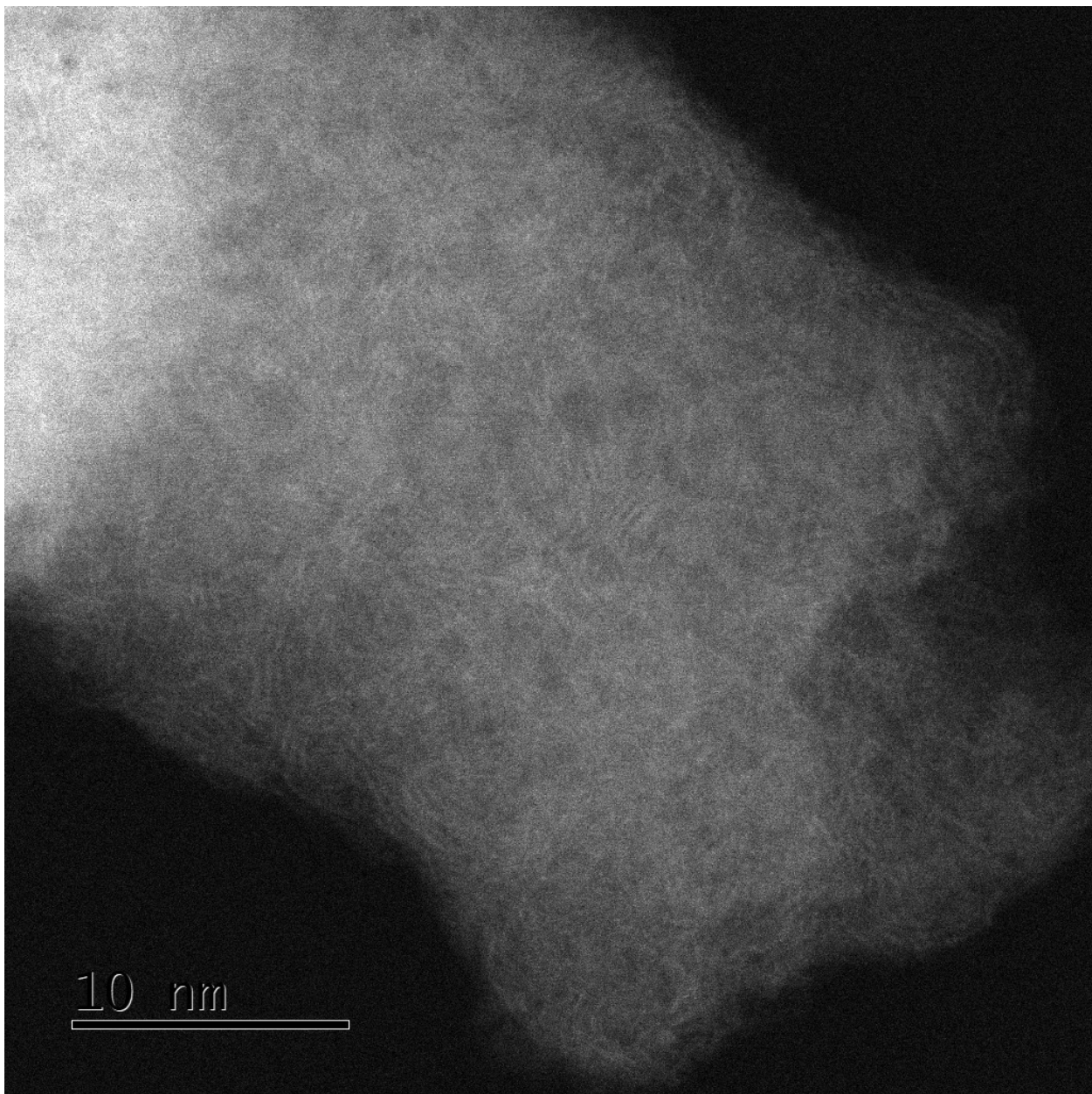


**Figure S6.** HAADF-STEM image of the catalyst after reaction.

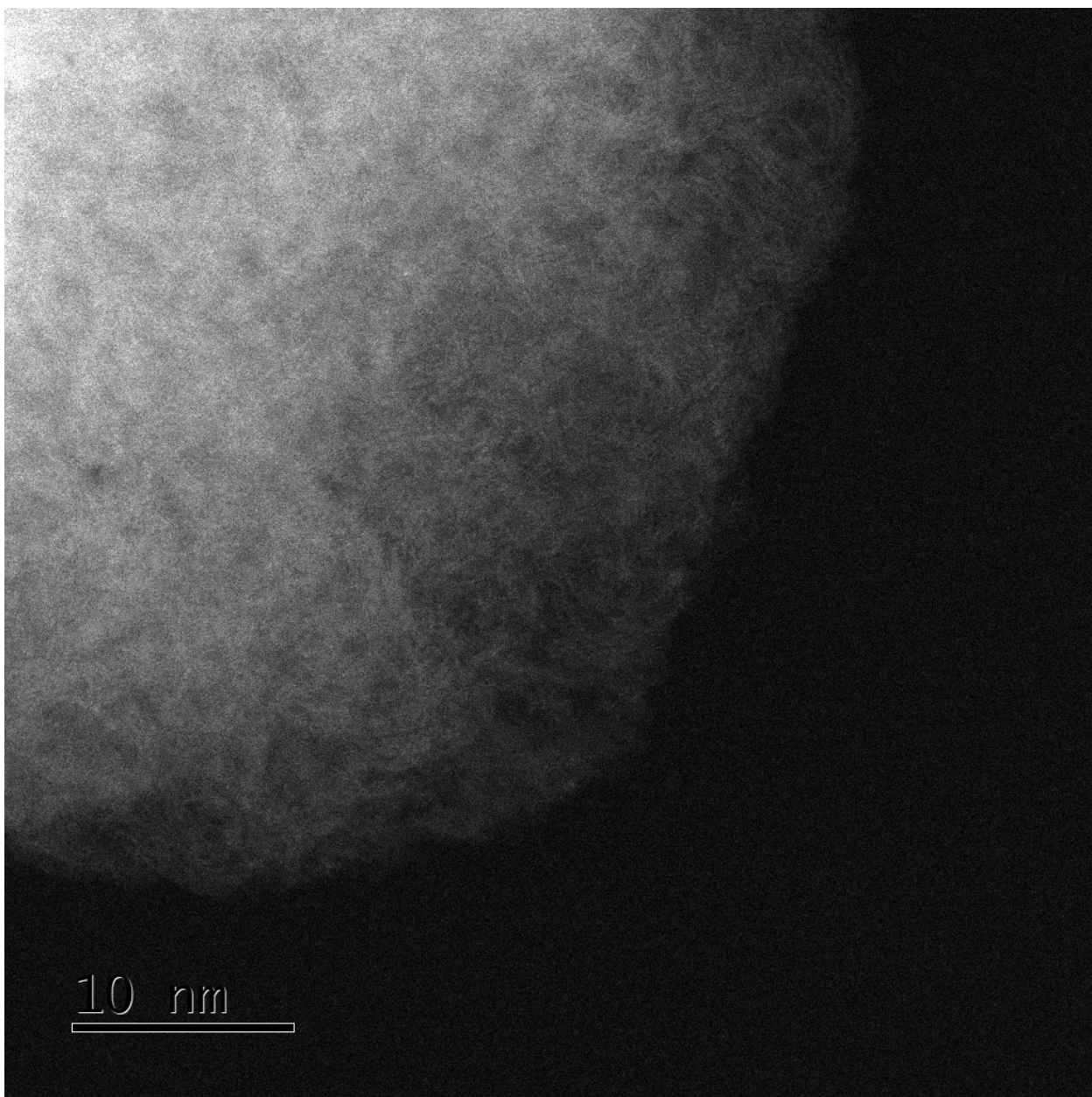


**Figure S7.** HAADF-STEM image of acid-washed catalyst (0.1 M HCl, room temperature, 16 h).

**Scanning electron microscope (SEM)** was conducted on Zeiss Leo Gemini 1525. High-resolution transmission electron microscopy was conducted on all the samples at an operating voltage of 300 kV. The samples were dispersed in ethanol and sonicated for 10 min, followed by casting onto lacey carbon mesh copper grids (Agar Scientific, Lacey carbon film 400 Cu). The grids were then placed in a vacuum desiccator to assist the evaporation of the solvent overnight before loading onto the SEM sample holder.

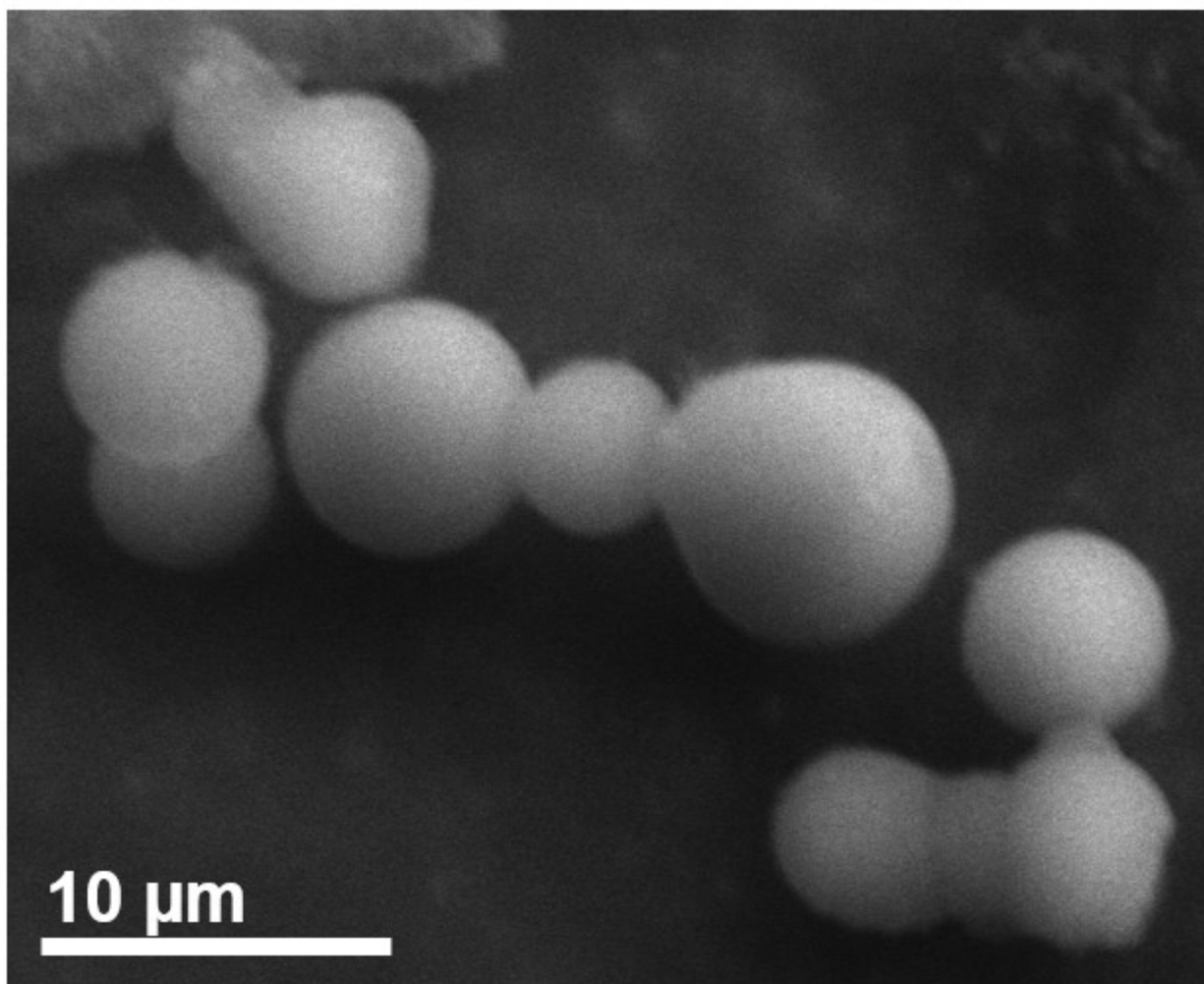


**Figure S8.** SEM image of the fresh catalyst.

**X-ray photoelectron spectroscopy (XPS)** analysis was conducted employing a Thermo Fisher K-Alpha XPS system, and the spectra were analysed with the Avantage software. All spectra were calibrated relative to the carbon C1s peak at 284.8 eV to correct charging effects.

Carbon species	Overall amount	Atomic %	Center peak shift (eV)
C=O	90.14	4.13	286.79
C-N		15.4	285.83
C-C		80.4	284.77
Nitrogen species	2.54	Atomic %	
Graphitic		61.7	401.13
Pyrrolic		12.7	399.68
Pyridinic		25.6	398.49

Oxygen species	7.57	Atomic %	
C=O		52.9	533.20
C-O		47.1	531.75

**Table S2.** XPS deconvolution details (Iron was detected at 0.5 at%)

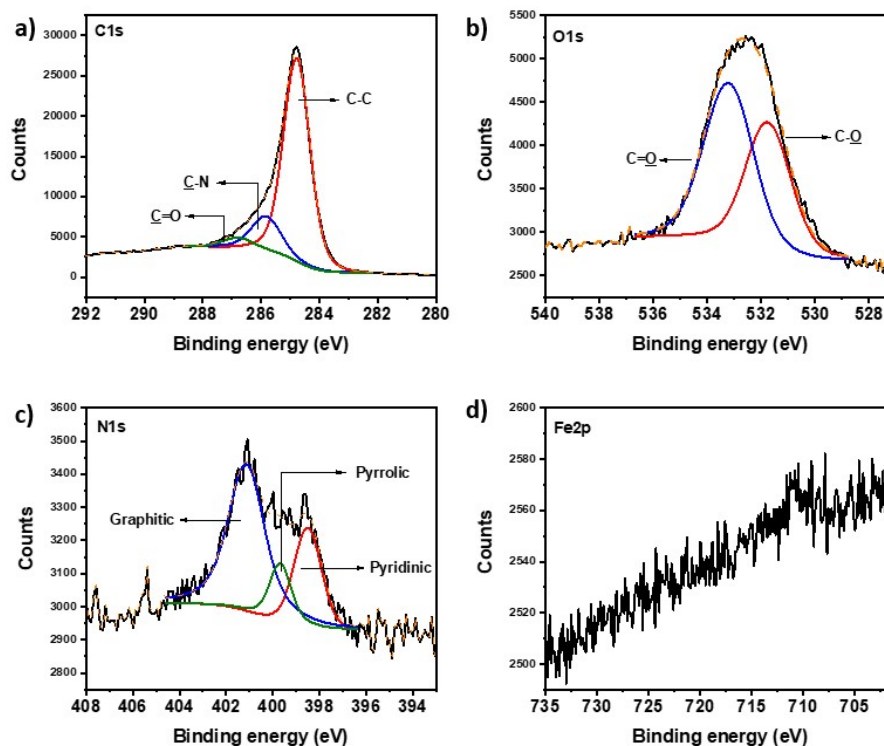


**Figure S9.** XPS of Fe<sub>N<sub>x</sub></sub>@C a) Carbon scan b) Nitrogen scan c) Oxygen scan d) Iron scan.

XRD patterns were obtained with a powder X-ray diffractometer (XRD PANanalytical's X'PERT PRO).

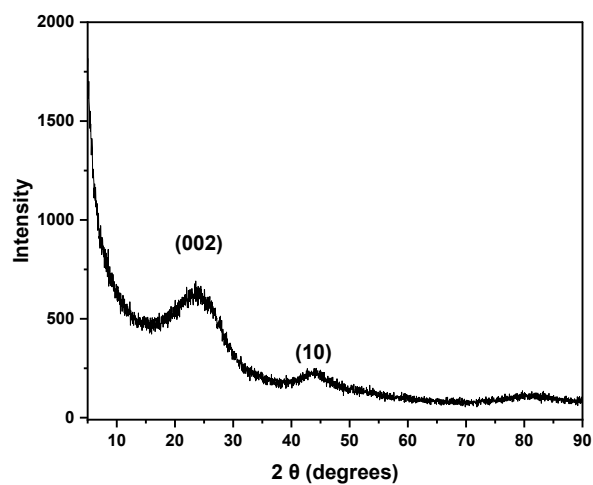


Figure S10. XRD of FeN<sub>x</sub>@C

Raman spectroscopy was used to analyse the defect structures of carbon materials using a Renishaw in Via Raman instrument with a laser wavelength of 532 nm, and the fitting of Raman spectra was based on the Lorentzian model.

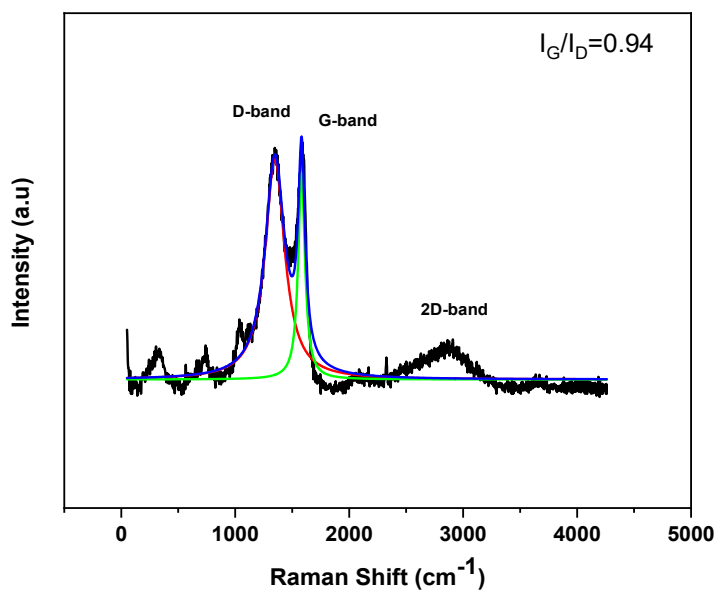


Figure S11. Raman spectrum of FeN<sub>x</sub>@C.

**X-ray absorption spectroscopy (XAS)** measurements were performed at beamline I20 of Diamond Light Source in fluorescence. Samples (~ 25 mg) were mixed with cellulose (~2-3 mg), pressed into pellet (50 mg cm<sup>-2</sup>), and sealed into Kapton tape for the XAS measurements. The data were normalised to the incident intensity and processed using the Athena software package.<sup>1</sup> A derivative ( $E_0$ ) value of 7112.0 eV corresponds to the first inflection point of the absorption K-edge. The measured EXAFS spectra were fit after subtracting pre-edge and post-edge background from the overall absorption and then normalizing with respect to the edge step. Subsequently, the  $\chi(k)$  data of 2.4 to 10 Å<sup>-1</sup> was used for the Fourier transformed data using a Hanning window (dk

= 1.0 Å<sup>-1</sup>) to separate the Extend X-ray absorption fine structure (EXAFS) contributions from different coordination shells around the absorbing Fe atom. Quantitative structural parameters around central atoms were fitted using ARTEMIS software.

Sample	Scattering pair	CN	R (Å)	ΔE0 (eV)	σ2 (10 <sup>-3</sup> Å <sup>2</sup> )	S02	R factor
FeN <sub>x</sub> @C	Fe-N	4.85	2.04	7.45 ± 1.41	4.00	1	1.58%
		±0.38	±0.01				
	Fe-C	2.10	2.35		4.00		
		±0.41	±0.01				
FeN <sub>x</sub> @C <sub>AR</sub>	Fe-N	5.95	1.91	3.83 ± 2.30	7.00	1	1.99%
		±0.48	±0.01				
	Fe-C	2.63	2.28		5.00		
		±0.81	±0.01				
	Fe-Fe	0.77	2.52		7.00		
		±0.32	±0.01				

Table S3. XAS fitting parameters

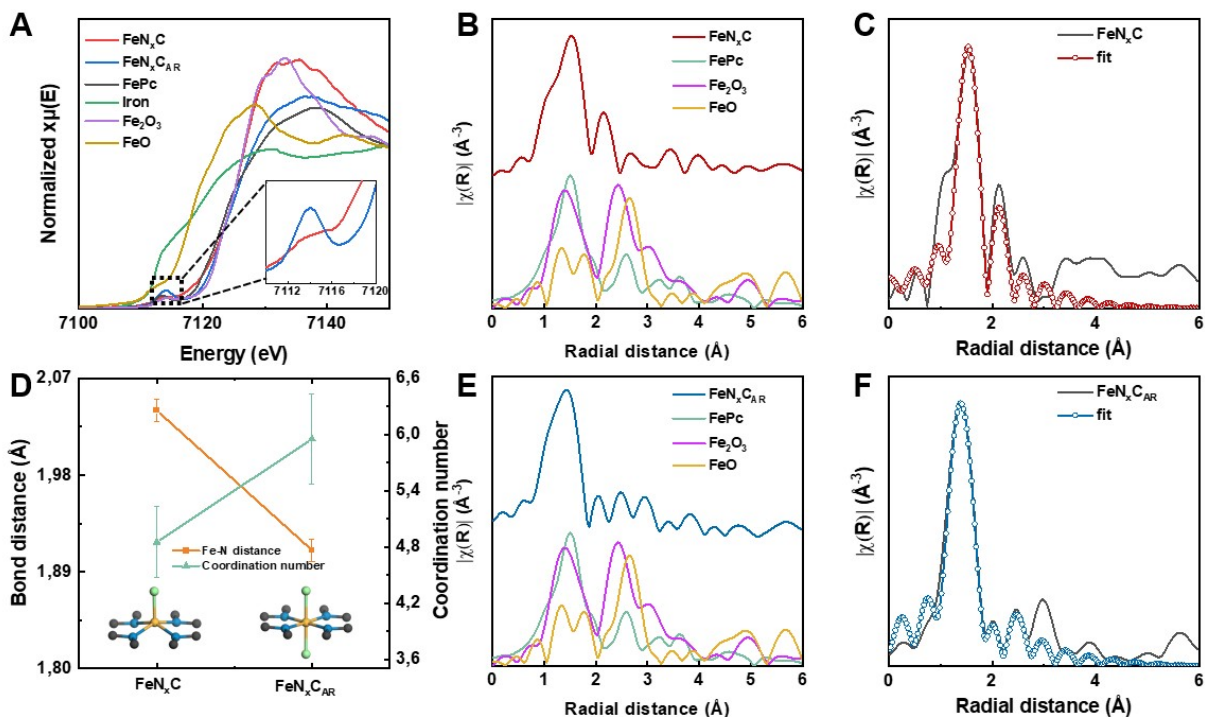


**Figure S12.** (a) XANES spectra of  $\text{FeN}_x\text{@C}$ ,  $\text{FeN}_x\text{@C}_{\text{AR}}$ ,  $\text{FePc}$ ,  $\text{Fe}_2\text{O}_3$ ,  $\text{FeO}$  and  $\text{Fe}$  foil. FT of Fe K-edge EXAFS spectra of  $\text{FeN}_x\text{@C}$  (b) and  $\text{FeN}_x\text{@C}_{\text{AR}}$  (e) compared to  $\text{FePc}$ ,  $\text{Fe}_2\text{O}_3$ ,  $\text{FeO}$  and  $\text{Fe}$  foil. Magnitude of EXAFS FT  $k^2$ -weight Fe K-edge spectra and fitting curve of (c)  $\text{FeN}_x\text{@C}$  and (f)  $\text{FeN}_x\text{@C}_{\text{AR}}$  (d) Comparison of bond length and coordination number before and after reaction. (proposed Fe-N structures where yellow spheres are iron, grey spheres are carbon, blue spheres are nitrogen, and green spheres are unknown ligand atoms).

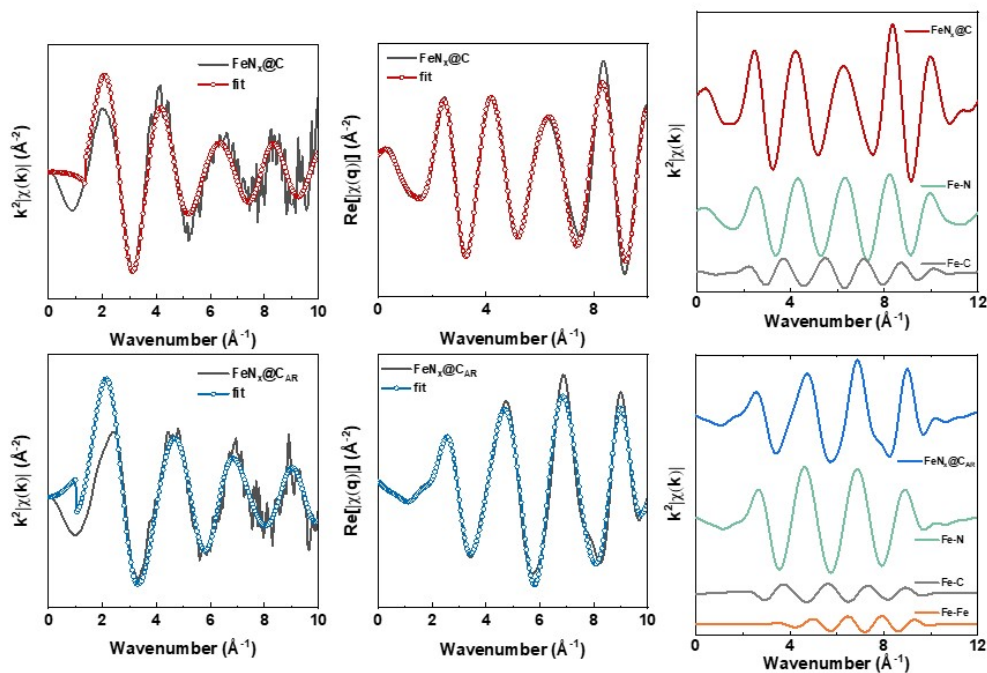


**Figure S13.** (a)  $k$ -space fitting curve of  $\text{FeN}_x\text{@C}$ , (b)  $q$ -space fitting curve of  $\text{FeN}_x\text{@C}$ , (c)  $q$ -space of  $\text{FeN}_x\text{@C}$  and Fe-N and Fe-C paths. (d) the  $k$ -space fitting curve of  $\text{FeN}_x\text{@C}_{\text{AR}}$ , (e)  $q$ -space fitting curve of  $\text{FeN}_x\text{@C}_{\text{AR}}$ , (f)  $q$ -space of  $\text{FeN}_x\text{@C}_{\text{AR}}$  and Fe-N, Fe-C, and Fe-Fe paths.

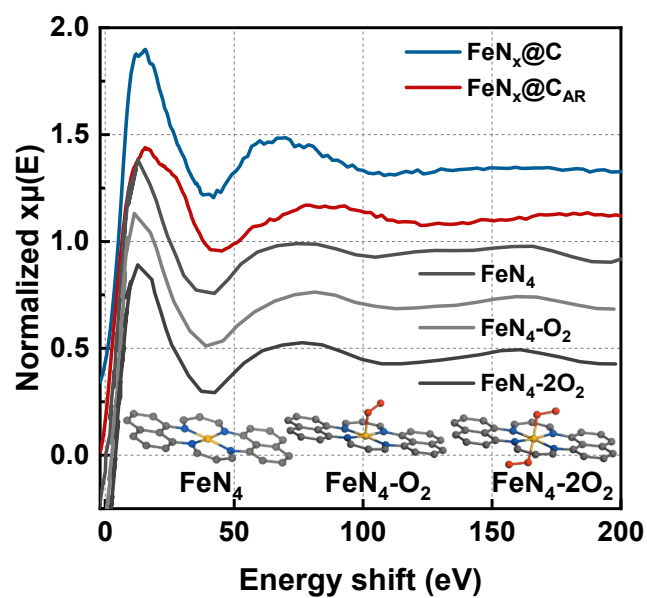


**Figure S14.** Comparison of XANES spectrums with the structure proposed by Zitolo *et al.*<sup>2</sup> (proposed Fe-N structures where yellow spheres are iron, grey spheres are carbon, blue spheres are nitrogen, and red spheres are oxygen)

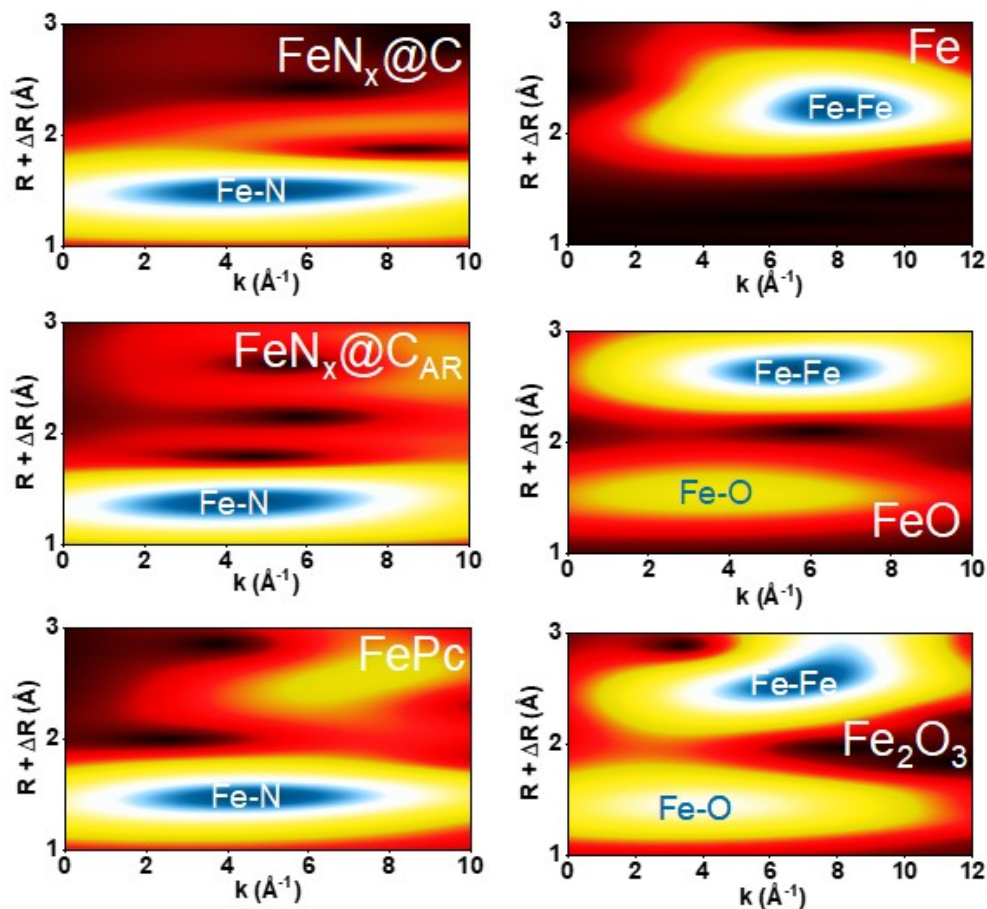


**Figure S15.** Wavelet transform of the  $k^2$ -weighted EXAFS data of  $\text{FeN}_x@C$ , Fe foil,  $\text{FeN}_x@C_{AR}$ , FePc, FeO and  $\text{Fe}_2\text{O}_3$ .

### 3-Catalysis

**Catalytic test.** Catalytic tests were conducted in Q-tubes (Q LabTech) purchased from Sigma Aldrich. Iron(II) phthalocyanine used in control reactions was purchased from Sigma-Aldrich (90% dye content), and was purified by sublimation before use.

In a typical catalytic test, the catalyst (50 mg) was loaded in an oven-dried Q-tube pressure reactor (12 mL) with 4-nitrotoluene (12 mg, 0.090 mmol),  $\text{K}_2\text{CO}_3$  (6 mg, 0.5 equiv.),  $\text{KCO}_2\text{H}$  (4 mg, 0.5 equiv.), isopropanol (2 mL), 1,3,5-trimethoxybenzene (5 mg) as an internal standard, and a PTFE-coated stirrer. The tube was capped with a septum, sonicated for 30 s and the mixture was purged with argon for 5 mins. The Q-tube was then sealed with a pressure cap (120 psi), before it was heated at 150 °C in a pre-heated oil bath. After 24 h, the pressure tube was cooled to room temperature and the septum was pierced with the safety needle. The reaction mixture was filtered through a celite plug, rinsed with methanol and ethyl acetate, then concentrated under vacuum. The residue was dissolved in  $\text{CDCl}_3$  and subjected to NMR analysis. The crude NMR yield was obtained from the integrals of the standard and products. Every entry was made in duplicate.

**Turnover frequency calculation.** TOF ( $\text{h}^{-1}$ ) was calculated in Table 1 as follows (assuming every Fe atom is catalytically active):

$$TOF = \frac{n_{prod}}{t \times m_{cat} \times \frac{[Fe]}{M_{Fe}}}$$

Where  $n_{prod}$  is the molar amount of toluidine formed (mmol),  $t$  the reaction time (24 h),  $m_{cat}$  the weight of catalyst introduced (50 mg),  $[Fe]$  the iron concentration in the material (%) and  $M_{Fe}$  the atomic weight of Fe (55.8 mg.mmol<sup>-1</sup>)

**Failed substrates.** In the case of 4-nitrobenzaldehyde and trans- $\beta$ -nitrostyrene, reduction was unsuccessful as neither the starting material nor the product were recovered after reaction (Figure S16). We believe polymerisation occurred in our catalytic conditions due to the presence in both cases of a bright yellow-orange product in the final product that was insoluble for  $^1\text{H-NMR}$  analysis.

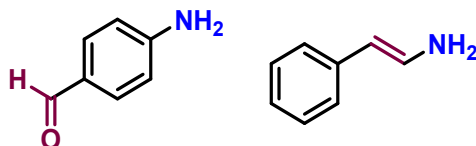


Figure S16. Failed nitroarene reduction substrate scope.

#### Optimization of 2-phenylbenzimidazole synthesis.

Entry	Deviation from standard conditions		Yield (%)
1	-		64
2	Solvent	Toluene	39
5	Additive	K <sub>2</sub> CO <sub>3</sub>	18
6	(1 equiv.)	NH <sub>4</sub> CO <sub>2</sub> H	62
Standard reaction conditions: 2-nitroaniline (13.8 mg, 0.1 mmol), benzyl alcohol (42 $\mu\text{L}$ , 4 eq.), acetonitrile (2 mL), Ar, 150°C, 24h.			

Table S4. Optimisation of 2-phenylbenzimidazole synthesis.

**Recycling tests.** For post-reaction metal analysis and catalyst reuse, celite filtration is not desirable since it can contaminate the material with traces of Fe (2 wt% in celite). Instead, the catalyst can be reused by centrifugation using a MeOH/2-MeTHF 1/10 volumetric mixture. The mixture was swirled and sonicated for 1 minute, then centrifuged at 10,000 rpm, 5 mins, repeated three times, allowing almost full recovery (99%) of the black powder. It was dried under vacuum overnight before reuse.

**Notes on water traces.** The reaction does not require to be prepared in dry conditions, though adding amounts of H<sub>2</sub>O as low as 5% (v/v) in isopropanol shut down the reaction completely. It is recommended to dry the catalyst, K<sub>2</sub>CO<sub>3</sub> and KCO<sub>2</sub>H, since they absorb water over time. After 6 months on the shelf, the catalyst gave a strong yield drop (down to 15% for the standard conditions), though the activity got restored after washing it with acetone and drying it at 80°C in the vacuum oven overnight.

**Comments on the mechanism.** Depending on the catalyst and the reductant used, nitroarene reduction can follow two pathways: direct or indirect (Figure S17).<sup>3</sup> For instance, Ni/ $\gamma$ -Al<sub>2</sub>O<sub>3</sub><sup>4</sup> works through the direct pathway where the nitro- group gets reduced to nitroso-, followed by the hydroxylamine, then to the corresponding amine. For other systems such as Pd/C with H<sub>2</sub>,<sup>5</sup> azoxy- condensates are formed, then get reduced to azo- and hydrazine intermediates before the final N-N cleavage to the amine.

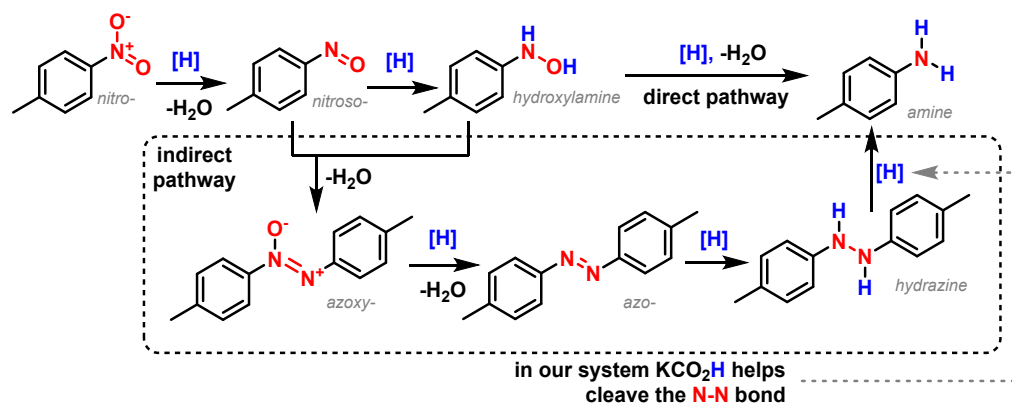
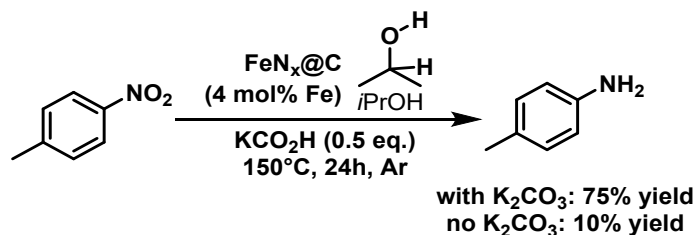


Figure S17. Mechanistic pathways for nitroarene reduction.

During our optimisation for 4-nitrotoluene reduction, we detected in the crude NMR mixture the presence of the hydrazine intermediate, indicating that  $\text{FeN}_x\text{@C}$  can perform at least all the steps through the indirect pathway. We further investigated the effects of both  $\text{K}_2\text{CO}_3$  and  $\text{KCO}_2\text{H}$  additives (Figure S18). Taking our standard conditions as a reference, removing the base decreased the yield from 75% to 10% of amine, although with no other intermediate detected (Figure S18a). Removing  $\text{KCO}_2\text{H}$  did not drastically decrease the overall conversion (around 70%), but this time half of the product formed was the hydrazine intermediate (Figure S18b). Altogether, we believe the role of the base is to help the catalyst perform the early steps of nitro reduction whereas  $\text{KCO}_2\text{H}$  is crucial for the N-N cleavage step.

a) role of  $\text{K}_2\text{CO}_3$



b) role of  $\text{KCO}_2\text{H}$

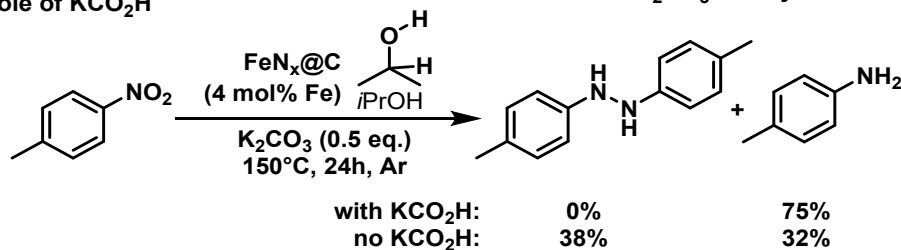
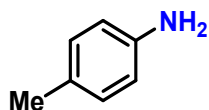


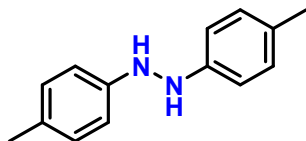
Figure S18. Role of  $\text{K}_2\text{CO}_3$  and  $\text{KCO}_2\text{H}$  in nitroarene reduction.

#### 4-NMR spectra

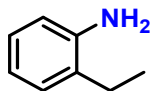
NMR spectra were recorded with a Jeol (1H, 400 MHz) spectrometer.



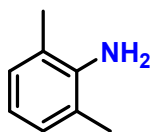
*Para*-toluidine.  $^1\text{H-NMR}$  (400 MHz,  $\text{CDCl}_3$ , ppm): 6.98 (d, 2H,  $J = 8.0$  Hz), 6.7 (d, 2H,  $J = 8.0$  Hz), 2.23 (s, 3H)



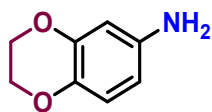
**1,2-di-*p*-tolylhydrazine.**<sup>6</sup> <sup>1</sup>H-NMR (400 MHz, CDCl<sub>3</sub>, ppm): 7.01 (d, 2H, J = 8.0 Hz), 6.74 (d, 2H, J = 8.0 Hz), 2.04 (s, 6H)



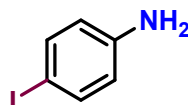
**2-ethylaniline.** <sup>1</sup>H-NMR (400 MHz, CDCl<sub>3</sub>, ppm): 7.05 (d, 1H, J = 7.6 Hz), 7.02 (t, 1H, J = 7.6 Hz), 6.75 (t, 1H, J = 7.6 Hz), 6.67 (d, 1H, J = 7.7 Hz), 2.52 (q, 2H, J = 7.2 Hz), 1.21 (t, 3H, J = 7.2 Hz)



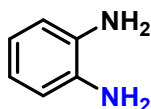
**2,6-Xylidine.** <sup>1</sup>H-NMR (400 MHz, CDCl<sub>3</sub>, ppm): 6.86 (d, 2H, J = 8.0 Hz), 6.59 (d, 1H, J = 8.0 Hz), 2.16 (s, 6H)



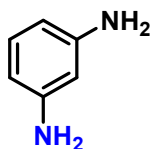
**1,4-Benzodioxan-6-amine.** <sup>1</sup>H-NMR (400 MHz, CDCl<sub>3</sub>, ppm): 6.68 (d, 1H, J = 8.4 Hz), 6.24 (d, 1H, J = 2.4 Hz), 6.22-6.19 (dd, 1H, J = 8.4 and 2.4 Hz), 4.23-4.17 (m, 4H)



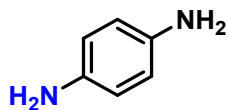
**4-Iodaniline.**<sup>7</sup> <sup>1</sup>H-NMR (400 MHz, CDCl<sub>3</sub>, ppm): 7.71 (d, 2H, J = 8.8 Hz), 6.48 (d, 2H, J = 8.8 Hz)



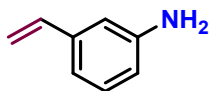
**Ortho-phenylenediamine.** <sup>1</sup>H-NMR (400 MHz, CDCl<sub>3</sub>, ppm): 6.71 (d, 2H, J = 7.6 Hz), 6.08 (d, 2H, J = 7.6 Hz)



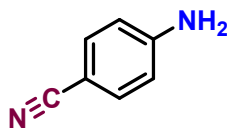
**Meta-phenylenediamine.** <sup>1</sup>H-NMR (400 MHz, CDCl<sub>3</sub>, ppm): 6.93 (t, 1H, J = 8.0 Hz), 6.11 (dd, 2H, J = 8.0 Hz and 2.4 Hz), 6.04 (t, 1H, J = 2.4 Hz)



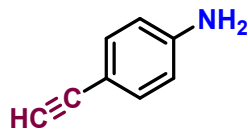
**Para-phenylenediamine.** <sup>1</sup>H-NMR (400 MHz, CDCl<sub>3</sub>, ppm): 6.57 (s, 4H)



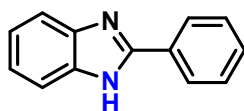
**3-aminostyrene.** <sup>1</sup>H-NMR (400 MHz, CDCl<sub>3</sub>, ppm): 7.14 (t, 1H, J = 8 Hz), 6.83 (d, 1H, J = 7.6 Hz), 6.76 (s, 1H), 6.63 (dd, 1H, J = 17.6 and 11.2 Hz), 6.62 (d, 1H, J = 8 Hz), 5.70 (dd, 1H, J = 17.6 and 1.2 Hz), 5.20 (dd, 1H, J = 11.2 and 0.8 Hz)



**4-aminobenzonitrile.**<sup>8</sup> <sup>1</sup>H-NMR (400 MHz, CDCl<sub>3</sub>, ppm): 7.42 (d, 2H, J = 8.4 Hz), 6.08 (d, 2H, J = 8.4 Hz)



**4-ethynylaniline.** NMR (400 MHz, CDCl<sub>3</sub>, ppm): 7.29 (td, 2H, J = 8.8 and 2.4 Hz), 6.58 (td, 2H, J = 8.8 and 2.4 Hz), 2.95 (s, 1H)



**2-Phenylbenzimidazole**<sup>9</sup> <sup>1</sup>H-NMR (400 MHz, DMSO, ppm): 8.19-8.17 (td, 2H, J = 6.8 and 1.6 Hz), 7.63-7.45 (m, 5H), 7.24-7.20 (m, 2H), 3.39 (broad, 1H).

- 1 B. Ravel and M. Newville, *Journal of Synchrotron Radiation*, 2005, **12**, 537–541.
- 2 A. Zitolo, V. Goellner, V. Armel, M.-T. Sougrati, T. Mineva, L. Stievano, E. Fonda and F. Jaouen, *Nature Materials*, 2015, **14**, 937–942.
- 3 A. Mahata, R. K. Rai, I. Choudhuri, S. K. Singh and B. Pathak, *Physical Chemistry Chemical Physics*, 2014, **16**, 26365–26374.
- 4 X. Meng, H. Cheng, Y. Akiyama, Y. Hao, W. Qiao, Y. Yu, F. Zhao, S. Fujita and M. Arai, *Journal of Catalysis*, 2009, **264**, 1–10.
- 5 E. A. Gelder, S. D. Jackson and C. M. Lok, *Chemical Communications*, 2005, 522–524.
- 6 L. Wang, A. Ishida, Y. Hashidoko and M. Hashimoto, *Angewandte Chemie International Edition*, 2017, **56**, 870–873.
- 7 J. Iskra, S. Stavber and M. Zupan, *Synthesis (Stuttgart)*, 2004, 1869–1873.
- 8 X. Cui, Q. Zhang, M. Tian and Z. Dong, *New Journal of Chemistry*, 2017, **41**, 10165–10173.
- 9 J. Y. Hao, Z. Y. Ge and S. Y. Yang, *Synthetic Communications*, 2003, **33**, 79–86.